Simulations of stent artifacts in Magnetic Resonance Imaging

Yan Guo, Xiaohua Jiang
Department of Electrical Engineering, Tsinghua University
3-316, West-Main Building, Tsinghua University, 100084, Beijing, China
jiangxiaohua@mail.tsinghua.edu.cn

Abstract —This paper presents an approach to simulate the stent artifacts in magnetic resonance imaging (MRI) based on electromagnetic (EM) analysis. Both static and radiofrequency (RF) field distributions with a sample stent in a uniform imaging phantom are calculated using the commercial finite element method (FEM) software JMAG 10.0. The images with stent artifacts are simulated by an MRI simulator according to the calculated field distributions.

I. INTRODUCTION

Metallic stents composed of paramagnetic materials, such as stainless steel, Ni-Ti alloy and Co-Cr alloy, etc., are widely used to treat arterial occlusive diseases [1]. However, these metallic implants cause artifacts in MR images due to magnetic susceptibility and RF field shielding [1-3].

As it is known, the local difference in susceptibility between the metallic implants and its surroundings perturbs the spatial uniformity of the static magnetic field (B0), while the RF field (B1) shielding impacts both the exciting RF field and the receiving sensitivity.

This paper proposes a method to simulate the stent artifacts in MRI according to 3D numerical EM analysis.

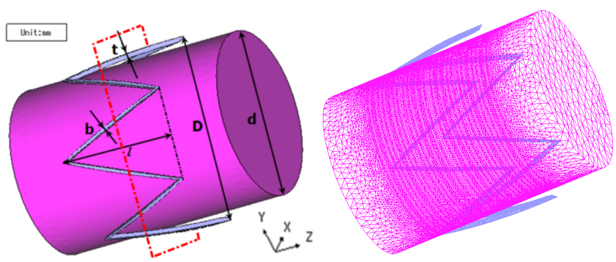

Fig. 1. Geometry and meshing of the sample stent (gray region) and ROI (red region), t=0.2mm, b=0.1mm, l=5mm, D=8mm, d=7.2mm.

II. METHODS

The geometries of the sample stent and the region of interest (ROI) in the imaging phantom are shown in Fig. 1. Two kinds of stent materials, 316L stainless steel (σ = 1.35×10^{6} S/m, χ= 9×10^{-3}) and Ni-Ti alloy (σ = 1.22×10^{6} S/m, χ= 3.1×10^{-4}), are used. The phantom (σ = 0.8 S/m, χ= -9.1×10^{-6}) is a cylinder of 40mm diameter and 40mm length. The mesh sizes of the model are listed in Table I, and the numbers of total nodes and elements are 216113 and 1270732 respectively. The mesh size in the stent is smaller than the skin depth to take into consideration the skin effect.

The static magnetic field distribution is simulated using the 3D static magnetic analysis module of JMAG. The simulation condition is an external static field of unit tesla.

Owing to the magnetic susceptibility, the fields of the areas that are close to the stent will be distorted causing the static field inhomogeneous. The unit local B0 distribution $\mathcal{B}_0(\vec{r})$ is the simulated magnetic flux density along the direction of the external static field. $\vec{r}$ is the spatial location.

The 3D frequency response analysis module of JMAG is performed to simulate the RF field distribution due to the quasi-static approximation. The simulation condition is an external RF filed of unit tesla (rms) rotating surrounding the direction of the B0 field.

As the external RF field will induce eddy currents in the metallic stent, the RF fields of the areas close to the stent will also be distorted causing the RF field inhomogeneous. If B0 is in the direction of axis Z, the unit local exciting field $\overrightarrow{\mathcal{B}_1}(\vec{r})$and receiving sensitivity $R(\vec{r})$ are given by,

$$\overrightarrow{\mathcal{B}_1}(\vec{r}) = B_{1x,unit}(\vec{r})\vec{\imath} + B_{1y,unit}(\vec{r})\vec{\jmath} \quad (1)$$

$$R(\vec{r}) = B_{1x,unit}(\vec{r}) + iB_{1y,unit}(\vec{r}) \quad (2)$$

where $B_{1x,unit}$ and $B_{1y,unit}$ are the simulated local magnetic flux densities (rms) along axis X and Y respectively..

TABLE I
MESH SIZES OF THE MODEL

Material	Regions	Element size
Ni-Ti / 316L	All	50um
Phantom	Radius: 0~3.6mm; Length: 10mm	0.5mm
	Radius: 3.6~4.2mm; Length: 6mm	0.1mm
	Radius: 3.6~10mm; Length: 20mm	2mm
	Radius: 10~20mm; Length: 40mm	4mm

The distortion of both the static and RF fields will cause artifacts in the MR images of the stent. An MRI simulator is used to simulate the stent artifacts that is based on the 3D Block equation in the rotating frame given by [4],

$$\frac{\mathrm{d}\vec{M}}{\mathrm{d}t} = \gamma\vec{M}\times\vec{B} - \frac{M_x\vec{\imath} + M_y\vec{\jmath}}{T_2} - \frac{(M_z - M_0)\vec{k}}{T_1} \quad (3)$$

where M_0 is the spin magnetization equilibrium value, the magnetization vector $\vec{M} = M_x\vec{\imath} + M_y\vec{\jmath} + M_z\vec{k}$, T_1 and T_2 are the relaxation constants and γ is the gyromagnetic constant. The local magnetic field $\vec{B}$ is given by,

$$\vec{B}(\vec{r},t) = B_0\Delta\mathcal{B}_0(\vec{r})\vec{k} + \left(\vec{G}(t)\cdot\vec{r}\right)\vec{k} + B_{rf}(t)\overrightarrow{\mathcal{B}_1}(\vec{r}) \quad (4)$$

where B_0 is the static main field, $\Delta\mathcal{B}_0(\vec{r}) = \mathcal{B}_0(\vec{r}) - 1$, $\vec{G}(t)$ is the applied field gradient, and $B_{rf}(t)$ is the exciting RF pulse shown in Fig.2.

During RF pulses, the block equation is solved using the Cayley-Klein parameters to simulate the shielding effect on the exciting RF field [5].

The received signal S(t) is calculated by [4],

$$S(t) = \int R^*(\vec{r})M_{xy}(\vec{r},t)\,\mathrm{d}\vec{r} \quad (5)$$

where $M_{xy} = M_x + iM_y$, and $R^*(\vec{r})$ is the complex conjugate of $R(\vec{r})$.

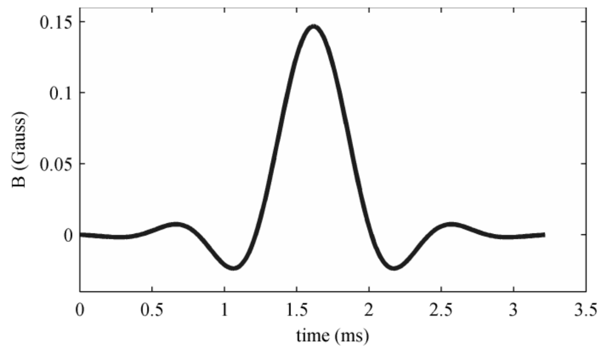

Fig. 2. RF pulse waveform

III. Results

A. Artifacts by B0 distortion

An external B0 of unit tesla along axis Z (symmetric axis of ROI) is applied. The stents made of 316L and Ni-Ti alloy are simulated respectively. The B0 distributions in the transversal center planes (illustrated by the dashed line in Fig.1) of ROI are shown in Fig. 3. The field inhomogeneity in ROI is 120ppm for 316L and 10ppm for Ni-Ti alloy, while the inhomogeneity in the transversal plane of the sample is 7.87ppm for 316L and 0.34ppm for Ni-Ti alloy. With a B0 of 0.3T, the simulated images of the transversal plane are acquired, as shown in Fig. 4, with a perfectly homogenous RF field of 12.77MHz, using a gradient-recalled echo (GRE) sequence with flip angle = 90°, TE = 30 ms, FOV = 5 cm × 5 cm, 128×128 imaging matrix, slice thickness = 1 mm. It can be seen that the stent made of Ni-Ti alloy causes smaller artifacts compared with those by 316L, which has larger magnetic susceptibility.

B. Artifacts by B1 distortion

An external B1 of unit tesla (rms) rotating at the resonance frequency of 12.77MHz is applied. The Ni-Ti alloy stent is simulated with B1 rotating surrounding axis Z and X respectively. The B1 distributions in the transversal plane of ROI are shown in Fig. 5. The simulated images, shown in Fig. 6, are acquired with a perfectly homogenous B0 field of 0.3T, using a spin echo (SE) sequence with TE = 30 ms, FOV = 5 cm × 5 cm, 128×128 imaging matrix, slice thickness = 1 mm. More serious B1 field inhomogeneity is caused when B1 is rotating surrounding axis X, resulting in larger coupling between B1 and the conductive loop of the stent. However, no significant difference between two images can be observed.

IV. Conclusion

A method of simulation of stent artifacts in MRI is developed based on electromagnetic field analysis. By an MRI simulator the simulated images with the stent artifacts are acquired. The results indicate that the stent made of Ni-Ti alloy with a small magnetic susceptibility is promising for obtaining the inside information without significant distortion while the stent of 316L seems difficult to look inside in MRI.

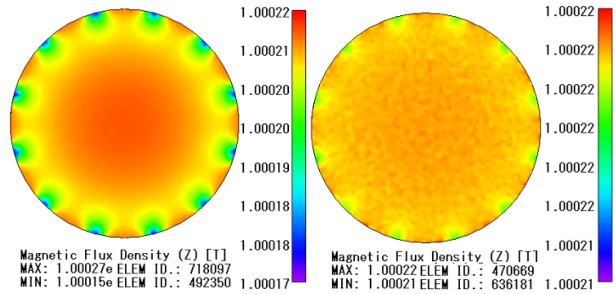

Fig. 3. B0 maps in transversal plane of ROI (left: 316L; right: Ni-Ti)

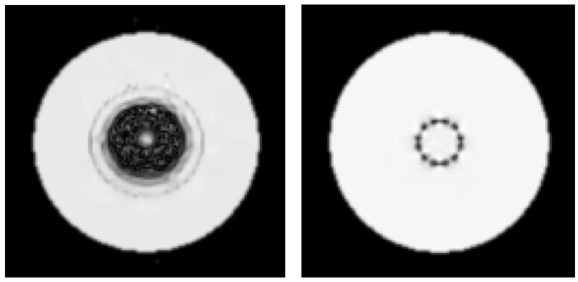
Fig. 4. Simulated images of GRE sequence (left: 316L; right: Ni-Ti)

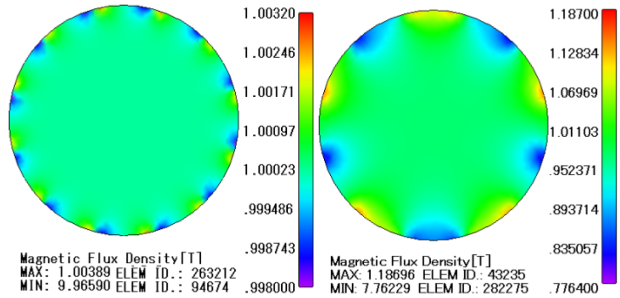

Fig. 5. B1 maps in transversal plane of ROI (left: B1 rotating surrounding axis Z; right: B1 rotating surrounding axis X)

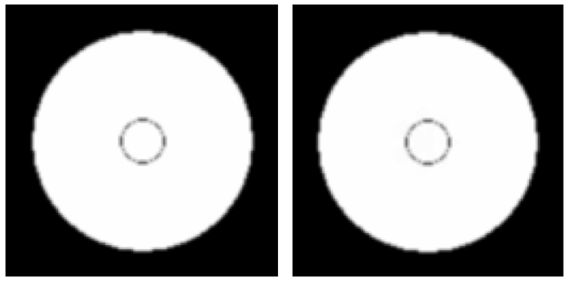
Fig. 6. Simulated images of SE sequence (left: B1 rotating surrounding axis Z; right: B1 rotating surrounding axis X)

V. References

[1] Yi Wang and T. N. Truong, "Quantitative evaluation of susceptibility and shielding effects of nitinol, platinum, cobalt-alloy, and stainless steel stents," Magn. Reson. Med., vol.49, pp. 972-976, 2003.
[2] Y. Gao, "Reduction of Artifact of Metallic Impant in Magnetic Resonance Imaging by Coating of Diamagnetic Material," IEEE Trans. on Magn., vol.45, no.10, pp. 4837-4840, 2009.
[3] L. W. Bartels, "Improved lumen visualization in metallic vascular implants by reducing RF artifacts," Magn. Reson. Med., vol.47, pp. 171-180, 2002.
[4] Zhi-Pei Liang and P.C. Lauterber, Principles of Magnetic Resonace Imaging: A Signal Processing Perspective, New York: IEEE Press, 2000, pp. 76-100
[5] J. Pauly, "A Linear Class of Large-Tip-Angle Selective Excitation Pulses," J. Magn. Reson., vol.82, pp. 571-587, 1989